ℓ_0-Norm Minimization based Robust Matrix Completion Approach for MIMO Radar Target Localization

Zhaofeng Liu, Xiao Peng Li, and Hing Cheung So, *Fellow, IEEE*

Abstract—In this paper, we propose a robust matrix completion approach based on ℓ_0-norm minimization for target localization in sub-Nyquist sampled multiple-input multiple-output (MIMO) radar. Owing to the low-rank property of the noise-free MIMO radar transmit matrix, our approach is able to recover the missing data and resist impulsive noise from the receive matrix. We adopt proximal block coordinate descent and adaptive penalty parameter adjustment by complex Laplacian kernel and normalized median absolute deviation. We analyze the resultant algorithm convergence and computational complexity, and demonstrate through simulations that it outperforms existing methods in terms of pseudospectrum, mean square error, and target detection probability in non-Gaussian impulsive noise, even for the full sampling schemes. While in the presence of Gaussian noise, our approach performs comparably with other sub-Nyquist methods.

Index Terms—target localization; MIMO radar; low-rank matrix completion; ℓ_0-norm minimization; impulsive noise; mean square error; target detection probability.

I. INTRODUCTION

Multiple-input multiple-output (MIMO) radar has attracted much attention from researchers [1]–[3]. Since colocated antennas provide waveform diversity, the target localization resolution of colocated MIMO radar is high [4]. In target localization, direction-of-arrival (DOA) estimation of incoming wave is essential. Moreover, it is assumed that the DOA of interested incoming wave is distinct within $-90°$ to $90°$, and may originate from only a few isolated directions. Therefore, the DOA can be estimated by sparse signal processing techniques like compressed sensing (CS) [5]–[8] which discretizes the non-linear model to a sparse solution vector. Since full data sampled with Nyquist rate are required in CS, the sampling load of electronic components is high.

In order to reduce the sampling load, researchers have considered sampling the receive pulse in a sampling rate less than Nyquist rate [9]–[13]. However, the data obtained by under-sampling are incomplete, further processing is needed to

recover the full data. To achieve this goal, matrix completion (MC) based MIMO radar is proposed [14]–[21]. When the number of antennas, the length of Nyquist sampling sequence and the number of pulses are significantly larger than the number of targets, the noise-free transmitted data matrix is of low-rank. Furthermore, low-rank MC can achieve noise reduction.

Most of the existing MC approaches for colocated MIMO radar is under an assumption that the additive noise obeys independent and identical Gaussian distribution. In fact, non-Gaussian impulsive noise [22], [23] widely appears in radar [24] and communication systems [25]–[27]. Comparing with Gaussian noise, the non-Gaussian noise has heavier tails in the probability distribution function (PDF). The heavier tails result in larger probability of outliers, and the power of outliers is as many times as the power of Gaussian noise, which dominates the overall noise power. Since the Gaussian noise usually has white spectrum, the MC for resisting Gaussian noise cannot suppress outliers properly. Therefore, the performance of colocated MIMO-MC radar designed for the Gaussian noise is remarkably degraded in impulsive noise. Recently, many approaches are proposed to enhance the outlier-resistance performance. The work of [28] solves a least absolute deviation problem by message passing to suppress outliers, while [29] uses the discrete Fourier transform to perform a joint Doppler frequency and DOA estimation for the MIMO radar affected by outliers. Moreover, to restrain outliers, [30] proposes a kernel minimum entropy based estimator, and [31] uses a Kalman filter. However, all of these methods do not utilize the low-rank property of MIMO radar signals and require the full data, which still result in huge sampling load.

In this paper, utilizing the low-rank property of colocated MIMO radar signal, we propose an ℓ_0-norm minimization MC approach to recover the radar signal from under-sampled incomplete data and enhance the outlier-resistance performance. We adopt ℓ_0-norm in MC to detect and suppress outliers. Our formulation of MC is a sum of Frobenius norm for reducing the Gaussian noise and ℓ_0-norm for suppressing outliers. To solve the resultant problem, proximal block coordinate descent (BCD) is utilized to decompose it into three sub-problems which can be alternately solved. Moreover, complex Laplacian kernel and median absolute deviation are applied to detect outliers. Thanks to the under-sampling and MC, the proposed approach works in a low mean square error (MSE) and high target detection probability without the requirement of full data. Simulation results show that comparing with the

conventional colocated MIMO-MC radar [16] designed for the Gaussian noise, the proposed approach has superior outlier-resistance performance in impulsive noise environment.

Our main contributions are summarized as:

1) To reduce the sampling load and enhance the robustness, an ℓ_0-norm minimization based MC approach is proposed for colocated MIMO radar target localization in possibly impulsive noise environment. Our MC approach is formulated using a sum of Frobenius norm and ℓ_0-norm. In doing so, the dense Gaussian noise is handled by the Frobenius norm while the sparse outliers are resisted by the ℓ_0-norm.

2) Proximal BCD with an proximal parameter is adopted to decompose the resultant formulation of our approach into Gaussian-resistance and outlier detection problems. Moreover, complex Laplacian kernel with joint PDF of the real and imaginary parts and normalized median absolute deviation are applied to detect outliers.

3) We have analyzed the convergence behavior of the devised method. That is, the objective function value is convergent, while the variable sequence converges to a local minimizer. Moreover, the algorithm complexity is included to demonstrate its computational attractiveness. The rationale behind the choice of the sampling scheme is also provided.

4) We perform simulations to verify the superior performance of the proposed approach. Its fast convergence speed is first demonstrated. Besides, in Gaussian mixture model (GMM) noise, the proposed method achieves better performance than the method with full data and Frobenius norm based approaches [16] in terms of pesudospectrum, MSE and target detection probability. Moreover, in Gaussian noise, the performance of the proposed approach is comparable to that of counterpart approaches designed for Gaussian noise.

The rest of the paper is organized as follows. Section II describes the background. The proposed ℓ_0-norm minimization based MC approach for MIMO radar target localization is presented in Section III. Subsequently, we analyze its convergence and complexity in Section IV, and simulation results are provided in Section V. Finally, Section VI concludes the paper.

II. BACKGROUND

In this section, notations and the basic colocated MIMO radar model are presented.

A. Notations

Let $(\cdot)^T$ and $(\cdot)^H$ denote the transpose and Hermitian transpose, respectively. Besides, $\mathbb{R}$ and $\mathbb{C}$ signify the real and complex spaces, respectively. For a complex number, $j = \sqrt{-1}$ is the imaginary unit and $|\cdot|$ denotes the magnitude. Moreover, $\Re(\cdot)$ and $\Im(\cdot)$ represent the real and imaginary parts of a complex number, respectively. In addition, $\otimes$ is the Kronecker product, $\circ$ denotes the element-by-element multiplication, $\mathrm{diag}(\cdot)$ transforms a vector to a diagonal matrix, and $\mathrm{vec}(\cdot)$ reshapes a matrix to a column vector. Furthermore,

$\mathrm{Prob}(\cdot)$ defines the probability of an event, $\mathbb{E}\{\cdot\}$ calculates the expectation, and $\max(\cdot)$ takes the maximum value.

B. Colocated MIMO Radar
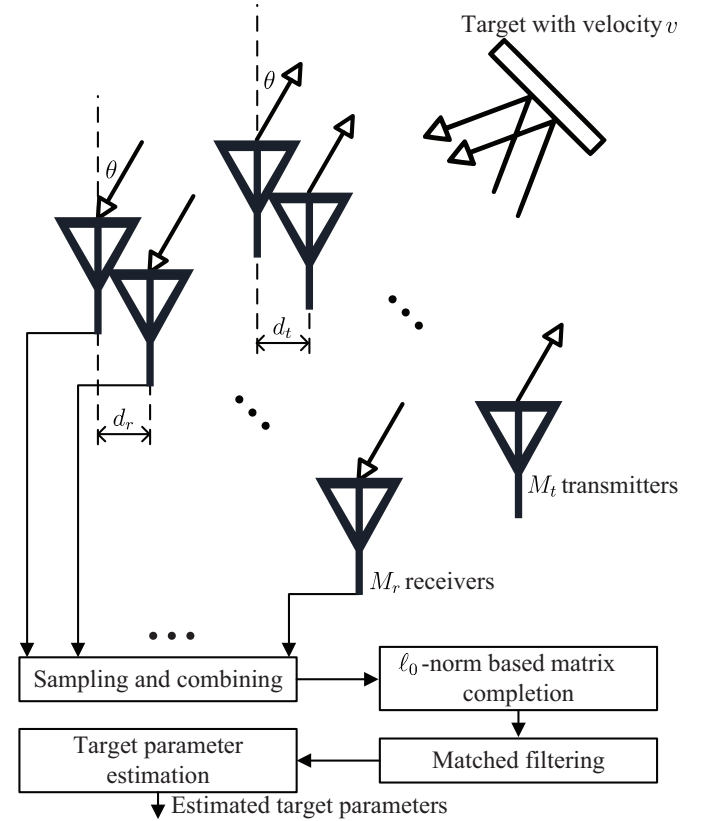
Fig. 1. Block diagram of the ℓ_0-norm based colocated MIMO radar system

Figure 1 shows the block diagram of the proposed colocated MIMO radar system based on ℓ_0-norm. In this subsection, the background of the colocated MIMO radar is introduced.

1) Transceiver: Consider a colocated MIMO radar system with M_t transmit antennas and M_r receive antennas in uniform linear array (ULA) setting for detecting K targets in the far field at distinct angles $\{\theta_k\}_{k=1}^{K}$ [16]. The inter-element spacings between transmit and receive antennas are d_t and d_r, respectively. To avoid phase ambiguity, it requires $d_t \leq \lambda/2$ and $d_r \leq \lambda/2$, where $\lambda = c/f_c$ is wavelength, f_c is the carrier frequency and $c = 3 \times 10^8$ m/s is the speed of light.

At the transmitter, Hadamard pulses are emitted by M_t antennas with a duration of T_p. Hardmard pulses have good correlation properties, which provide high resolution to radar and allow signal transmission from multiple antennas without interference. Moreover, Hadamard pulses have simple structures, allowing easy implementation by hardware. The continuous Hadamard pulses can be sampled as discrete Hadamard code. In this system, the Hadamard code has the length of $N = 128$, and one Hadamard code used for one transmit antenna can be represented as a row in complex Hadamard matrix $\boldsymbol{H}_N^c \in \mathbb{C}^{N \times N}$, given by:

$$\boldsymbol{H}_N^c = \frac{1+j}{\sqrt{2N}}\boldsymbol{H}_N, \ \boldsymbol{H}_N = \boldsymbol{H}_2 \otimes \boldsymbol{H}_{N/2} \qquad (1)$$

where $\boldsymbol{H}_2 = [1, \ 1; 1, \ -1]$. Since only M_t antennas transmit the pulses, the first M_t rows of $\boldsymbol{H}_N^c$ describe all transmit pulses, denoted as $\boldsymbol{S} \in \mathbb{C}^{M_t \times N}$. After transmitting a pulse, the transmit antennas are turned off for detection, and the same pulse is transmitted repeatedly. Here, the interval between successive pulses is T_{PRI}, and the number of repeat times is Q. Since the transmit antennas are arranged in ULA, its transmit steering vector for the kth target at θ_k is [16]:

$$\boldsymbol{a}(\theta_k) = [1, e^{j\frac{2\pi}{\lambda}d_t \sin(\theta_k)}, \cdots, e^{j\frac{2\pi}{\lambda}(M_t-1)d_t \sin(\theta_k)}]^T \quad (2)$$

where $k = 1, \cdots, K$. Subsequently, all transmit steering vectors construct the transmit steering matrix as $\boldsymbol{A} = [\boldsymbol{a}(\theta_1), \cdots, \boldsymbol{a}(\theta_K)]$.

The channel fading is included in the system model of bistatic uniform linear array MIMO radar [32], with $\boldsymbol{\Gamma}_q$ and $\boldsymbol{D}_q$ representing the target reflection coefficient and Doppler spread, respectively [33]. The qth pulse transmitted to the kth target is affected by the Doppler spread $d_{q,k}$ and the target reflection coefficient $\gamma_{q,k}$ [34]. We assume that the transmitted waveform is narrowband, which means that the waveform bandwidth $1/T_p$ is much smaller than the carrier frequency f_c. The narrowband pulse assumption also induces that the transmitted waveform suffers from flat fading, and the delay spread at the receiver is much smaller than T_p. We also presume that the Doppler spread of the signal reflected by the kth target is much smaller than the pulse bandwidth, given by $2v_k/\lambda \ll 1/T_p$, where v_k is the velocity of the kth target [16]. The Doppler spread $d_{q,k} = e^{j(2\pi/\lambda)2v_k(q-1)T_{\mathrm{PRI}}}$ constructs a matrix $\boldsymbol{D}_q = \mathrm{diag}(\boldsymbol{d}_q)$ where $\boldsymbol{d}_q = [d_{q,1}, \cdots, d_{q,K}]^T$. Moreover, the target reflection coefficient follows the Swerling II model [35], and forms a matrix $\boldsymbol{\Gamma}_q = \mathrm{diag}(\boldsymbol{\gamma}_q)$ where $\boldsymbol{\gamma}_q = [\gamma_{q,1}, \cdots, \gamma_{q,K}]^T$. In addition to the above multiplicative fading, the signal suffers from Gaussian noise or impulsive noise in the wireless channel.

At the receiver, the receive steering vector for the kth target at θ_k is:

$$\boldsymbol{b}(\theta_k) = [1, e^{j\frac{2\pi}{\lambda}d_r \sin(\theta_k)}, \cdots, e^{j\frac{2\pi}{\lambda}(M_r-1)d_r \sin(\theta_k)}]^T. \quad (3)$$

Subsequently, all receive steering vectors construct the receive steering matrix as $\boldsymbol{B} = [\boldsymbol{b}(\theta_1), \cdots, \boldsymbol{b}(\theta_K)]$.

2) Matched Filter: Before further processing, the discrete data points are sampled from the received waveform. If the sampling interval is the Nyquist sampling period T_s, N data points are sampled from one pulse, which is represented as a row in the receive matrix $\boldsymbol{R}_q \in \mathbb{C}^{M_r \times N}$ of the form:

$$\boldsymbol{R}_q = \boldsymbol{Z}_q + \boldsymbol{W}_q = \boldsymbol{B}\boldsymbol{\Gamma}_q\boldsymbol{D}_q\boldsymbol{A}^T\boldsymbol{S} + \boldsymbol{W}_q \quad (4)$$

where $\boldsymbol{Z}_q = \boldsymbol{B}\boldsymbol{\Gamma}_q\boldsymbol{D}_q\boldsymbol{A}^T\boldsymbol{S}$ is a low-rank matrix, and $\boldsymbol{W}_q$ is the noise matrix. Here, the low-rank property of $\boldsymbol{Z}_q$ is due to the fact that $\boldsymbol{\Gamma}_q\boldsymbol{D}_q$ is a $K \times K$ diagonal matrix and the assumption that M_r and N are much larger than K.

In [16], two sampling schemes are proposed to sample the signal. The first performs matched filtering before mixing all received signals together, and the second applies reverse processing. We choose the second scheme for better outlier-resistance performance, and the reason of this choice can be found in Appendix A. For one pulse, a receive antenna can

sample at most N samples in the Nyquist sampling period T_s. Specifically, the antenna samples the pulse at times nT_s, where $n = 0, 1, \cdots, N-1$. To reduce the load of sampling, only a small number of elements in $\boldsymbol{R}_q$ are sampled. The receive antenna samples the pulse only at specific times $n'T_s$, where $n' \in \mathcal{J}^l$, and $\mathcal{J}^l$ is a random number set that contains $N_l < N$ distinct integers in $[0, N-1]$. The integers in $\mathcal{J}^l$ denote the sampling instants of the lth receive antenna.

After sampling, the samples and the index set $\mathcal{J}^l$ are passed to the combiner shown in Fig. 1, which constructs an N-length vector by inserting zeros into the samples according to $\mathcal{J}^l$. All N-length vectors from M_r receive antennas are collected to construct $\boldsymbol{R}_{q,\Omega} = \boldsymbol{R}_q \circ \boldsymbol{\Omega}_q$, where $\boldsymbol{\Omega}_q \in \mathbb{R}^{M_r \times N}$ is a matrix consisting of 0 and 1 randomly, and the indices of 1 in the lth row are elements in $\mathcal{J}^l$. To design $\boldsymbol{\Omega}_q$, a pre-defined proportion of 1s, which is named the observation rate O_r, is used to determine its number in $\boldsymbol{\Omega}_q$. The lower bound of O_r has been investigated in [16]. Moreover, $\boldsymbol{\Omega}_q$ cannot have a row or column whose entries are all 0s. After under-sampling, $\boldsymbol{R}_{q,\Omega}$ with all $q = 1, \cdots, Q$ are gathered and reshaped as one matrix for further processing, denoted as:

$$\begin{aligned}\boldsymbol{R}_\Omega &= [\mathrm{vec}(\boldsymbol{R}_{1,\Omega}), \cdots, \mathrm{vec}(\boldsymbol{R}_{Q,\Omega})] \\ &= [\mathrm{vec}(\boldsymbol{R}_1), \cdots, \mathrm{vec}(\boldsymbol{R}_Q)] \circ [\mathrm{vec}(\boldsymbol{\Omega}_1), \cdots, \mathrm{vec}(\boldsymbol{\Omega}_Q)] \\ &= \boldsymbol{R} \circ \boldsymbol{\Omega} = (\boldsymbol{Z} + \boldsymbol{W}) \circ \boldsymbol{\Omega}\end{aligned}$$

$$(5)$$

where

$$\begin{aligned}\boldsymbol{R} &= [\mathrm{vec}(\boldsymbol{R}_1), \cdots, \mathrm{vec}(\boldsymbol{R}_Q)] \\ \boldsymbol{\Omega} &= [\mathrm{vec}(\boldsymbol{\Omega}_1), \cdots, \mathrm{vec}(\boldsymbol{\Omega}_Q)] \\ \boldsymbol{Z} &= [\mathrm{vec}(\boldsymbol{Z}_1), \cdots, \mathrm{vec}(\boldsymbol{Z}_Q)] \\ \boldsymbol{W} &= [\mathrm{vec}(\boldsymbol{W}_1), \cdots, \mathrm{vec}(\boldsymbol{W}_Q)] \\ \boldsymbol{R} &= \boldsymbol{Z} + \boldsymbol{W} \quad (6)\end{aligned}$$

where $\boldsymbol{W}$ is the reshaped noise matrix. Subsequently, the robust ℓ_0-norm minimization based MC is applied to $\boldsymbol{R}_\Omega$ to recover the matrix and resist outliers. For better recovery performance of MC, $\boldsymbol{Z}$ should be of low-rank, which is proved in Appendix B. Details of the robust ℓ_0-norm minimization based MC are presented in Section III.

3) Target Parameter Estimation: The multiple signal classification (MUSIC) [36] based algorithm is applied to estimate the DOAs of K targets thanks to its compatibility with MC and acceptable complexity. Denoting the MC recovered matrix as $\hat{\boldsymbol{Z}} \in \mathbb{C}^{M_r N \times Q}$, the output of the matched filter is:

$$\hat{\boldsymbol{Z}}_{MF} = (\bar{\boldsymbol{S}} \otimes \boldsymbol{I}_{M_r})\hat{\boldsymbol{Z}} \quad (7)$$

where $\bar{\boldsymbol{S}}$ is the complex conjugate of $\boldsymbol{S}$, and $\boldsymbol{I}_{M_r}$ is the $M_r \times M_r$ identity matrix. According to [16], the covariance matrix of $\hat{\boldsymbol{Z}}_{MF} \in \mathbb{C}^{M_t M_r \times Q}$ should be calculated first, which is:

$$\hat{\boldsymbol{C}} = \frac{1}{Q}\hat{\boldsymbol{Z}}_{MF}\hat{\boldsymbol{Z}}_{MF}^H. \quad (8)$$

Afterwards the pseudospectrum is given by [16]:

$$P(\theta) = \frac{1}{(\boldsymbol{a}(\theta) \otimes \boldsymbol{b}(\theta))^H \boldsymbol{E}_n \boldsymbol{E}_n^H (\boldsymbol{a}(\theta) \otimes \boldsymbol{b}(\theta))}, \ |\theta| < 90°$$

$$(9)$$

where $\boldsymbol{E}_n$ contains all eigenvectors of the noise subspace of $\hat{\boldsymbol{C}}$. The MUSIC-based algorithm finds the peaks in the pseudospectrum, then the corresponding values of θ are the estimated DOAs of targets.

III. ℓ_0-NORM MINIMIZATION ALGORITHM

In this section, we introduce the ℓ_0-norm minimization based MC algorithm.

Existing MC based algorithms for colocated MIMO radar do not consider the impulsive noise environment and they adopt the Frobenius norm to formulate the recovery problem, leading to:

$$\min_{\boldsymbol{U},\boldsymbol{V}} \ \|(\boldsymbol{U}\boldsymbol{V})_\Omega - \boldsymbol{R}_\Omega\|_F^2 \tag{10}$$

where $\|\cdot\|_F$ is the Frobenius norm. This formulation can be solved by QR factorization [37]–[39]. Although the Frobenius norm is effective for reducing Gaussian noise, it cannot obtain good performance in impulsive noise channels.

In the impulsive noise environment, outliers are sparsely distributed. To improve the performance in impulsive noise environment, we attempt to separate the sparse outliers from the noise, and exploit ℓ_0-norm penalty to suppress the outliers. Recalling (5), when the noise is impulsive, there exist outliers in noise matrix $\boldsymbol{W}$, thus $\boldsymbol{W}$ can be divided as Gaussian noise matrix $\boldsymbol{G}$ and outlier matrix $\boldsymbol{O}$. Therefore, (5) is rewritten as:

$$\boldsymbol{R}_\Omega = (\boldsymbol{Z}+\boldsymbol{W})\circ\boldsymbol{\Omega} = (\boldsymbol{Z}+\boldsymbol{G}+\boldsymbol{O})\circ\boldsymbol{\Omega} = \boldsymbol{Z}_\Omega+\boldsymbol{G}_\Omega+\boldsymbol{O}_\Omega. \tag{11}$$

We exploit the element-wise matrix ℓ_0-norm to detect the sparse outliers, and $\boldsymbol{O}$ is defined to store the detected outliers. The ℓ_0-norm is defined as the number of non-zero elements in a matrix, and it measures the sparsity of a matrix. That is, if ℓ_0-norm is applied to the observed matrix, it is able to separate sparse outliers from given data. We integrate the Frobenius norm and ℓ_0-norm together to resist the Gaussian noise and outliers at the same time. According to the definition of ℓ_0-norm and the expression of receive matrix (11), the proposed approach is:

$$\min_{\boldsymbol{U},\boldsymbol{V},\boldsymbol{O}} \|\boldsymbol{R}_\Omega - (\boldsymbol{U}\boldsymbol{V})_\Omega - \boldsymbol{O}_\Omega\|_F^2 + \mu\|\boldsymbol{O}_\Omega\|_0 \tag{12}$$

where $\mu > 0$ is a parameter to control the sparsity of $\boldsymbol{O}_\Omega = \boldsymbol{O}\circ\boldsymbol{\Omega}$. In (12), the Frobenius norm is used for reducing Gaussian noise and the ℓ_0-norm is used to identify and suppress outliers. Subsequently, in order to solve (12), proximal BCD [40] is adopted, resulting in the following three subproblems:

$$\boldsymbol{U}^{l+1} = \arg\min_{\boldsymbol{U}} \|\boldsymbol{R}_\Omega - (\boldsymbol{U}\boldsymbol{V}^l)_\Omega - \boldsymbol{O}_\Omega^l\|_F^2 + \frac{\phi}{2}\|\boldsymbol{U} - \boldsymbol{U}^l\|_F^2 \tag{13}$$

$$\boldsymbol{V}^{l+1} = \arg\min_{\boldsymbol{V}} \|\boldsymbol{R}_\Omega - (\boldsymbol{U}^{l+1}\boldsymbol{V})_\Omega - \boldsymbol{O}_\Omega^l\|_F^2 + \frac{\phi}{2}\|\boldsymbol{V} - \boldsymbol{V}^l\|_F^2 \tag{14}$$

$$\boldsymbol{O}^{l+1} = \arg\min_{\boldsymbol{O}} \|\boldsymbol{R}_\Omega - (\boldsymbol{U}^{l+1}\boldsymbol{V}^{l+1})_\Omega - \boldsymbol{O}_\Omega\|_F^2$$
$$+ \mu^{(l+1)}\|\boldsymbol{O}_\Omega\|_0 + \frac{\phi}{2}\|\boldsymbol{O}_\Omega - \boldsymbol{O}_\Omega^l\|_F^2 \tag{15}$$

where $\phi > 0$ is the pre-defined proximal parameter, l denotes the iteration number, and $\boldsymbol{O}_\Omega^l = \boldsymbol{O}^l \circ \boldsymbol{\Omega}$. Now μ is also considered as an unknown parameter to be estimated adaptively,

which is replaced by $\mu^{(l+1)}$. We first present the solutions for (13)–(15) as follows. It is observed that (13) can be decoupled in a row-by-row manner, then independent optimization of each row can be applied. Denote $\boldsymbol{Y}_\Omega^l = \boldsymbol{R}_\Omega - \boldsymbol{O}_\Omega^l$ and let $(\boldsymbol{y}_{\Omega_i}^l)^H$ be the vector storing the entries in the ith row of $\boldsymbol{Y}_\Omega^l$ with indices in Ω_i, where Ω_i is the index set of element "1" in the ith row of $\boldsymbol{\Omega}$. Similarly, we define $\boldsymbol{u}_i^H$ as the ith row of $\boldsymbol{U}$, and $\boldsymbol{V}_{\Omega_i}^l$ as the matrix consisting of columns in $\boldsymbol{V}^l$ with indices in Ω_i. Then (13) is equivalent to:

$$\boldsymbol{u}_i^{l+1} = \arg\min_{\boldsymbol{u}_i} \|\boldsymbol{y}_{\Omega_i}^l - (\boldsymbol{V}_{\Omega_i}^l)^H \boldsymbol{u}_i\|_2^2 + \frac{\phi}{2}\|\boldsymbol{u}_i - \boldsymbol{u}_i^l\|_2^2. \tag{16}$$

Analogously, considering (14) column-by-column, $\boldsymbol{v}_j^{l+1}$, the jth column of $\boldsymbol{V}^{l+1}$, is separately estimated from:

$$\boldsymbol{v}_j^{l+1} = \arg\min_{\boldsymbol{v}_j} \|\boldsymbol{y}_{\Omega_j}^l - \boldsymbol{U}_{\Omega_j}^{l+1}\boldsymbol{v}_j\|_2^2 + \frac{\phi}{2}\|\boldsymbol{v}_j - \boldsymbol{v}_j^l\|_2^2 \tag{17}$$

where Ω_j is the index set of element "1" in the jth column of $\boldsymbol{\Omega}$, while $\boldsymbol{U}_{\Omega_j}^{l+1}$ and $\boldsymbol{y}_{\Omega_j}^l$ contain rows in $\boldsymbol{U}^{l+1}$ and jth column of $\boldsymbol{Y}_\Omega^l$ with indices in Ω_j, respectively. Since (16) and (17) are linear least squares problems, the global solutions are straightforwardly calculated as:

$$(\boldsymbol{u}_i^{l+1})_* = (2\boldsymbol{V}_{\Omega_i}^l(\boldsymbol{V}_{\Omega_i}^l)^H + \phi\boldsymbol{I})^{-1}(2\boldsymbol{V}_{\Omega_i}^l\boldsymbol{y}_{\Omega_i}^l + \phi\boldsymbol{u}_i^l) \tag{18}$$

$$(\boldsymbol{v}_j^{l+1})_* = (2(\boldsymbol{U}_{\Omega_j}^{l+1})^H\boldsymbol{U}_{\Omega_j}^{l+1} + \phi\boldsymbol{I})^{-1}(2(\boldsymbol{U}_{\Omega_j}^{l+1})^H\boldsymbol{y}_{\Omega_j}^l + \phi\boldsymbol{v}_j^l) \tag{19}$$

For solving (15), we first define the difference of incomplete noise-contaminated matrix and recovered matrix at the $(l+1)$th iteration as:

$$\boldsymbol{E}_\Omega^{l+1} = \boldsymbol{R}_\Omega - (\boldsymbol{U}^{l+1}\boldsymbol{V}^{l+1})_\Omega. \tag{20}$$

Afterwards (15) becomes:

$$\boldsymbol{O}^{l+1} = \arg\min_{\boldsymbol{O}} \|\boldsymbol{E}_\Omega^{l+1} - \boldsymbol{O}_\Omega\|_F^2 + \mu^{(l+1)}\|\boldsymbol{O}_\Omega\|_0 + \frac{\phi}{2}\|\boldsymbol{O}_\Omega - \boldsymbol{O}_\Omega^l\|_F^2. \tag{21}$$

Vectorizing (21) and removing the unobserved entries yield:

$$\boldsymbol{o}^{l+1} = \arg\min_{\boldsymbol{o}} \|\boldsymbol{e}^{l+1} - \boldsymbol{o}\|_2^2 + \mu^{(l+1)}\|\boldsymbol{o}\|_0 + \frac{\phi}{2}\|\boldsymbol{o} - \boldsymbol{o}^l\|_2^2 \tag{22}$$

where $\boldsymbol{e}^{l+1}$ and $\boldsymbol{o}$ are vectors containing elements of $\boldsymbol{E}_\Omega^{l+1}$ and $\boldsymbol{O}_\Omega$ with indices in Ω in the column-first manner, respectively. Prior to solving (22), the value of $\mu^{(l+1)}$, which determines the sparsity of $\boldsymbol{O}_\Omega^{l+1}$ and the number of outliers at each iteration, is required. Therefore, in order to obtain $\mu^{(l+1)}$, outlier detection in $\boldsymbol{e}^{l+1}$ is needed and we use the complex Laplacian kernel, defined as [41]:

$$k_{\sigma_R,\sigma_I}(e_i^{l+1}) = \frac{1}{4\sigma_R\sigma_I}\exp\left(-\frac{|\Re(e_i^{l+1})|}{\sigma_R} - \frac{|\Im(e_i^{l+1})|}{\sigma_I}\right) \tag{23}$$

where e_i^{l+1} is the ith element of $\boldsymbol{e}^{l+1}$, σ_R and σ_I are bandwidths of $\Re(\boldsymbol{e}^{l+1})$ and $\Im(\boldsymbol{e}^{l+1})$, respectively. The complex Laplacian kernel is defined as the joint PDF of Laplace distributions with real and imaginary parts of e_i^{l+1}. The complex Laplacian kernel has the ability to detect outliers since it returns a small value when e_i^{l+1} has a large magnitude. In the kernel density estimation, the bandwidths are calculated

using the normalized median absolute deviation as [42]:

$$\sigma_R = 1.4826 \times \text{median}\left(\left|\Re\left(\boldsymbol{e}^{l+1}\right) - \text{median}\left(\Re\left(\boldsymbol{e}^{l+1}\right)\right)\right|\right) \tag{24}$$

$$\sigma_I = 1.4826 \times \text{median}\left(\left|\Im\left(\boldsymbol{e}^{l+1}\right) - \text{median}\left(\Im\left(\boldsymbol{e}^{l+1}\right)\right)\right|\right) \tag{25}$$

where $\text{median}(\cdot)$ denotes the sample median. When $k_{\sigma_R,\sigma_I}(e_i^{l+1}) \leq \epsilon$ where ϵ is a user-defined threshold, e_i^{l+1} is assigned as an outlier. Typically, ϵ is set as 10^{-3}. Defining $\mathcal{I}_{l+1}$ as the set of indices i corresponding to outliers $\{e_i^{l+1}\}$, $\mu^{(l+1)}$ is calculated as:

$$\mu^{(l+1)} = \min\left\{\left|e_1^{l+1}\right|^2, \cdots, \left|e_i^{l+1}\right|^2, \cdots, \left|e_{|\mathcal{I}_{l+1}|}^{l+1}\right|^2, \mu^{(l)}\right\} \tag{26}$$

where $|\mathcal{I}_{l+1}|$ is the cardinality of $\mathcal{I}_{l+1}$.

After obtaining $\mu^{(l+1)}$, (22) can be computed in an element-wise manner:

$$o_i^{l+1} = \arg\min_o \left|e_i^{l+1} - o\right|^2 + \mu^{(l+1)}I(o) + \frac{\phi}{2}\left|o - o_i^l\right|^2 \tag{27}$$

where $I(o) = 0$ when $o = 0$, $I(o) = 1$ when $o \neq 0$, o_i^{l+1} and o_i^l are the ith elements of $\boldsymbol{o}^{l+1}$ and $\boldsymbol{o}^l$, respectively. When $o = 0$, the value of the function in (27) is $\left|e_i^{l+1}\right|^2 + \phi\left|o_i^l\right|^2/2$, and when $o \neq 0$, the infimum of (27) is:

$$\inf_o \left|e_i^{l+1} - o\right|^2 + \mu^{(l+1)} + \frac{\phi}{2}\left|o - o_i^l\right|^2 = \mu^{(l+1)} + \frac{\phi\left|e_i^{l+1} - o_i^l\right|^2}{\phi + 2}. \tag{28}$$

The infimum exists when $o = (e_i^{l+1} + \phi o_i^l/2)/(1 + \phi/2)$. Therefore, $o \neq 0$ when the infimum is less than $\left|e_i^{l+1}\right|^2 + \phi\left|o_i^l\right|^2/2$, otherwise $o = 0$. Finally, we have:

$$o_i^{l+1} = \begin{cases} \dfrac{e_i^{l+1} + \frac{\phi o_i^l}{2}}{1 + \frac{\phi}{2}}, \\ \quad \text{if } \mu^{(l+1)} \leq \left|e_i^{l+1}\right|^2 + \dfrac{\phi\left|o_i^l\right|^2}{2} - \dfrac{\phi\left|e_i^{l+1} - o_i^l\right|^2}{\phi + 2}, \\ 0, \text{ otherwise.} \end{cases} \tag{29}$$

After all element-wise operations, the obtained $\boldsymbol{o}^{l+1}$ is reconstructed back to $\boldsymbol{O}_\Omega^{l+1}$ according to $\boldsymbol{\Omega}$. The overall procedure is summarized in Algorithm 1.

After ℓ_0-norm minimization, the MUSIC based target parameters estimation algorithm is applied to the resultant matrix $\hat{\boldsymbol{R}}$ for DOA estimation. Details of MUSIC can be found in Section II-B3.

IV. THEORETICAL ANALYSIS

A. Convergence

1) Non-increasing Objective Function Value: We first prove that the objective function value is non-increasing. Firstly, we add subscripts $\mu^{(l)}$ and $\mu^{(l+1)}$ in the objective function of (12) to denote its values at the lth and $(l+1)$th iterations, respectively. Then the difference of the objective function

---

Algorithm 1 Low-rank matrix recovery with ℓ_0-norm minimization

Input: $\boldsymbol{R}_\Omega$, $\boldsymbol{\Omega}$, $\epsilon = 10^{-3}$
  Initialize: Randomly initialize $\boldsymbol{U}^0$ and $\boldsymbol{V}^0$, $\boldsymbol{O}^0 = \boldsymbol{0}$, $\mu^{(0)} = \max(|R_{i,j}|^2)$.
  for $l = 0, 1, \ldots$ **do**
    for $n = 0, 1, \ldots, N - 1$ **do**
      Update $\boldsymbol{u}_i^{l+1}$ based on (18).
    end for
    for $k = 0, 1, \ldots, \beta - 1$ **do**
      Update $\boldsymbol{v}_j^{l+1}$ based on (19).
    end for
    Compute $\boldsymbol{E}_\Omega^{l+1} = \boldsymbol{R}_\Omega - (\boldsymbol{U}^{l+1}\boldsymbol{V}^{l+1})_\Omega$.
    Transform $\boldsymbol{E}_\Omega^{l+1}$ to $\boldsymbol{e}^{l+1}$.
    Compute σ_R and σ_I based on (24) and (25).
    Compute $k_{\sigma_R,\sigma_I}(e_i^{l+1})$ based on (23).
    Construct $\mathcal{I}_{l+1}$ which contains all indices i satisfying $k_{\sigma_R,\sigma_I}(e_i^{l+1}) \leq \epsilon$.
    Compute $\mu^{(l+1)}$ based on (26).
    Compute $\boldsymbol{o}^{l+1}$ based on (29).
    Construct $\boldsymbol{O}_\Omega^{l+1}$ with $\boldsymbol{o}^{l+1}$ and $\boldsymbol{\Omega}$.
    Stop when termination condition is met.
  end for
Output: $\hat{\boldsymbol{R}} = \boldsymbol{U}^{l+1}\boldsymbol{V}^{l+1}$

---

value in two adjacent iterations is written as:

$$\begin{aligned}
&f_{\mu^{(l+1)}}(\boldsymbol{U}^{l+1}, \boldsymbol{V}^{l+1}, \boldsymbol{O}^{l+1}) - f_{\mu^{(l)}}(\boldsymbol{U}^l, \boldsymbol{V}^l, \boldsymbol{O}^l) \\
&= \underbrace{f_{\mu^{(l)}}(\boldsymbol{U}^{l+1}, \boldsymbol{V}^l, \boldsymbol{O}^l) - f_{\mu^{(l)}}(\boldsymbol{U}^l, \boldsymbol{V}^l, \boldsymbol{O}^l)}_{f_1} \\
&\quad + \underbrace{f_{\mu^{(l)}}(\boldsymbol{U}^{l+1}, \boldsymbol{V}^{l+1}, \boldsymbol{O}^l) - f_{\mu^{(l)}}(\boldsymbol{U}^{l+1}, \boldsymbol{V}^l, \boldsymbol{O}^l)}_{f_2} \\
&\quad + \underbrace{f_{\mu^{(l+1)}}(\boldsymbol{U}^{l+1}, \boldsymbol{V}^{l+1}, \boldsymbol{O}^l) - f_{\mu^{(l)}}(\boldsymbol{U}^{l+1}, \boldsymbol{V}^{l+1}, \boldsymbol{O}^l)}_{f_3} \\
&\quad + \underbrace{f_{\mu^{(l+1)}}(\boldsymbol{U}^{l+1}, \boldsymbol{V}^{l+1}, \boldsymbol{O}^{l+1}) - f_{\mu^{(l+1)}}(\boldsymbol{U}^{l+1}, \boldsymbol{V}^{l+1}, \boldsymbol{O}^l)}_{f_4}
\end{aligned} \tag{30}$$

where f_1, f_2, f_3 and f_4 refer to the objective function differences after computing (13), (14), (26) and (15), respectively. Since $\boldsymbol{U}^{l+1}$, $\boldsymbol{V}^{l+1}$, and $\boldsymbol{O}^{l+1}$ are the optimal solutions of (13), (14), and (15), respectively, and (26) indicates $\mu^{(l+1)} \leq \mu^{(l)}$, all f_1, f_2, f_3 and f_4 are not greater than 0, implying that $f(\boldsymbol{U}, \boldsymbol{V}, \boldsymbol{O})$ is non-increasing.

2) Bounded Sequence: Since according to (30), the objective function value is non-increasing, we have $f_{\mu^{(l)}}(\boldsymbol{U}^l, \boldsymbol{V}^l, \boldsymbol{O}^l) \leq f_{\mu^{(0)}}(\boldsymbol{U}^0, \boldsymbol{V}^0, \boldsymbol{O}^0)$, which means that the objective function value after each iteration is upper bounded by $f_{\mu^{(0)}}(\boldsymbol{U}^0, \boldsymbol{V}^0, \boldsymbol{O}^0)$. Moreover, according to the property of norm, the objective function value is also lower bounded. Subsequently, if $\|\boldsymbol{U}_0\|_F, \|\boldsymbol{V}_0\|_F, \|\boldsymbol{O}_0\|_F, \mu^{(0)} < \infty$, we have $f_{\mu^{(0)}}(\boldsymbol{U}^0, \boldsymbol{V}^0, \boldsymbol{O}^0) < \infty$ and $f_{\mu^{(l)}}(\boldsymbol{U}^l, \boldsymbol{V}^l, \boldsymbol{O}^l) < \infty$. Therefore, when $l \rightarrow \infty$, $\|\boldsymbol{U}_l\|_F, \|\boldsymbol{V}_l\|_F, \|\boldsymbol{O}_l\|_F \rightarrow \infty$ is impossible since it contradicts $f_{\mu^{(l)}}(\boldsymbol{U}^l, \boldsymbol{V}^l, \boldsymbol{O}^l) < \infty$, which means that values of $\boldsymbol{U}^l, \boldsymbol{V}^l, \boldsymbol{O}^l$ are bounded. Furthermore, according to (26), $\mu^{(l)}$ is non-negative, and non-increasing

during the update. Hence we can also conclude that $\mu^{(l)}$ is bounded.

3) Convergence to local minimizer: To prove the local convergence, we show that the sequence $\{U^{l+1}, V^{l+1}, O^{l+1}\}$ generated by (13), (14), and (15) satisfies the following [43]:

$$\|R_\Omega - (U^{l+1}V^l)_\Omega - O_\Omega^l\|_F^2 + \frac{\phi}{2}\|U^{l+1} - U^l\|_F^2$$
$$\leq \|R_\Omega - (U^lV^l)_\Omega - O_\Omega^l\|_F^2 \quad (31)$$

$$\|R_\Omega - (U^{l+1}V^{l+1})_\Omega - O_\Omega^l\|_F^2 + \frac{\phi}{2}\|V^{l+1} - V^l\|_F^2$$
$$\leq \|R_\Omega - (U^{l+1}V^l)_\Omega - O_\Omega^l\|_F^2 \quad (32)$$

$$\|R_\Omega - (U^{l+1}V^{l+1})_\Omega - O_\Omega^{l+1}\|_F^2$$
$$+ \mu^{(l+1)}\|O_\Omega^{l+1}\|_0 + \frac{\phi}{2}\|O_\Omega^{l+1} - O_\Omega^l\|_F^2$$
$$\leq \|R_\Omega - (U^{l+1}V^{l+1})_\Omega - O_\Omega^l\|_F^2 + \mu^{(l+1)}\|O_\Omega^l\|_0$$
$$\leq \|R_\Omega - (U^{l+1}V^{l+1})_\Omega - O_\Omega^l\|_F^2 + \mu^{(l)}\|O_\Omega^l\|_0 \quad (33)$$

where the second inequality in (33) is deduced by the non-increasing property of μ given in (26). Subsequently, summing (31), (32), and (33) yields:

$$f_{\mu^{(l+1)}}(U^{l+1}, V^{l+1}, O^{l+1})$$
$$+ \frac{\phi}{2}\|U^{l+1} - U^l\|_F^2 + \frac{\phi}{2}\|V^{l+1} - V^l\|_F^2 + \frac{\phi}{2}\|O_\Omega^{l+1} - O_\Omega^l\|_F^2$$
$$= \|R_\Omega - (U^{l+1}V^{l+1})_\Omega - O_\Omega^{l+1}\|_F^2 + \mu^{(l+1)}\|O_\Omega^{l+1}\|_0$$
$$+ \frac{\phi}{2}\|U^{l+1} - U^l\|_F^2 + \frac{\phi}{2}\|V^{l+1} - V^l\|_F^2 + \frac{\phi}{2}\|O_\Omega^{l+1} - O_\Omega^l\|_F^2$$
$$\leq \|R_\Omega - (U^{l+1}V^{l+1})_\Omega - O_\Omega^l\|_F^2 + \mu^{(l)}\|O_\Omega^l\|_0$$
$$= f_{\mu^{(l)}}(U^l, V^l, O^l). \quad (34)$$

Then (34) is equivalent to:

$$\frac{\phi}{2}\|U^{l+1} - U^l\|_F^2 + \frac{\phi}{2}\|V^{l+1} - V^l\|_F^2 + \frac{\phi}{2}\|O_\Omega^{l+1} - O_\Omega^l\|_F^2$$
$$\leq f_{\mu^{(l)}}(U^l, V^l, O^l) - f_{\mu^{(l+1)}}(U^{l+1}, V^{l+1}, O^{l+1}). \quad (35)$$

Summing over $l = 0, 1, \cdots, L-1$ yields [44]:

$$\sum_{l=0}^{L-1} \frac{\phi}{2}\|U^{l+1} - U^l\|_F^2 + \frac{\phi}{2}\|V^{l+1} - V^l\|_F^2 + \frac{\phi}{2}\|O_\Omega^{l+1} - O_\Omega^l\|_F^2$$
$$\leq f_{\mu^{(0)}}(U^0, V^0, O^0) - f_{\mu^{(L)}}(U^L, V^L, O^L) < \infty \quad (36)$$

where $f_{\mu^{(0)}}(U^0, V^0, O^0)$ is a finite constant, and $f_{\mu^{(L)}}(U^L, V^L, O^L)$ is non-negative and bounded. Taking the limit as $L \to \infty$ in (36), we have [44]:

$$\lim_{l \to \infty} \frac{\phi}{2}\|U^{l+1} - U^l\|_F^2 + \frac{\phi}{2}\|V^{l+1} - V^l\|_F^2 + \frac{\phi}{2}\|O_\Omega^{l+1} - O_\Omega^l\|_F^2$$
$$= 0 \quad (37)$$

Subsequently, combining (37) and (20) leads to:

$$\lim_{l \to \infty} \|E_\Omega^{l+1} - E_\Omega^l\|_F^2 = 0. \quad (38)$$

Since $\mu^{(l+1)}$ is derived from elements in E_Ω^{l+1}, we can obtain from (38) that:

$$\lim_{l \to \infty} \left|\mu^{(l+1)} - \mu^{(l)}\right| = 0. \quad (39)$$

Combining (37), (39) and the bounded condition proved in Section IV-A2, we can conclude that (U^l, V^l, O^l) has a subsequence to converge. Moreover, according to [45], our objective function has the Kurdyka-Łojasiewicz (KL) property. Based on the subsequence convergence and the KL property, (U^l, V^l, O^l) converges to a local minimizer (U^*, V^*, O^*), see Theorem 2 of [40].

B. Computational Complexity

To solve (13) and (14), from (18) and (19) we know that the update of u_i^{l+1} has the complexity of $\mathcal{O}(|\Omega_i|K^2)$, and the update of v_j^{l+1} has the complexity of $\mathcal{O}(|\Omega_j|K^2)$. Therefore, both updates of U^{l+1} and V^{l+1} have the complexity of $\mathcal{O}(|\Omega|K^2)$ since $\sum_{i=1}^N |\Omega_i| = |\Omega|$ and $\sum_{j=1}^\beta |\Omega_j| = |\Omega|$. For (15), since the computation of complex Laplacian kernel is linear with the number of sampled elements, the complexity is $\mathcal{O}(|\Omega|)$. Therefore, the overall complexity of the ℓ_0-norm minimization algorithm is the sum of complexity for optimizing (13), (14) and (15), which is $\mathcal{O}(|\Omega|K^2)$. The complexity of the proposed algorithm is linear to $|\Omega|$. This implies that under-sampling can reduce the computational complexity of the MIMO radar system, making it suitable for systems with a large sampling load. Similarly, the complexity of the Frobenius norm based MC in (10) is also $\mathcal{O}(|\Omega|K^2)$, since (13) and (14) are still involved. The complexity comparison with other systems is presented in Table I, which shows that our system has low computational complexity.

TABLE I
COMPLEXITY COMPARISON

Approach	Complexity
Proposed	$\mathcal{O}(|\Omega|K^2)$
Frobenius norm based MC	$\mathcal{O}(|\Omega|K^2)$
Singular value thresholding based MC [16]	$\mathcal{O}(M_r NQ^2)$
ℓ_p-norm based MC [46]	$\mathcal{O}(|\Omega|N_{IRLS}K^2)$

The Frobenius norm based MC, [16], and the ℓ_0-norm minimization algorithm are realized using a PC with Intel i7-9700 3.00GHz CPU. The execution time of the Frobenius norm based MC, [16], and the ℓ_0-norm minimization algorithm are 2.59s, 6.26s, and 2.76s, respectively. The results show that the ℓ_0-norm minimization algorithm is much faster than [16], and has similar execution time as that of the Frobenius norm based MC.

V. SIMULATION RESULTS

Parameters of our simulation study are listed in Table II, where O_r denotes the ratio of sampled data points to the maximum number of data points. For the impulsive noise, GMM is a popular model whose PDF is:

$$p_w(w) = \frac{c_1}{\pi\sigma_1^2}e^{-\frac{|w|^2}{\sigma_1^2}} + \frac{c_2}{\pi\sigma_2^2}e^{-\frac{|w|^2}{\sigma_2^2}} \quad (40)$$

where both c_1 and c_2 are in $(0, 1)$, $c_1 + c_2 = 1$, σ_1^2 and σ_2^2 are the variances of Gaussian components. Without the loss

TABLE II
SYSTEM PARAMETERS

Parameter	Value
Number of transmit antennas	$M_t = 10$
Number of receive antennas	$M_r = 10$
Number of targets	$K = 2$
Wavelength	$\lambda = 0.3$m
Spacing of transmit antennas	$d_t = \lambda/2$
Spacing of receive antennas	$d_t = \lambda/2$
Number of pulses	$Q = 128$
Pulse length	$N = 128$
Pulse repetition interval	$T_{\mathrm{PRI}} = 5 \cdot 10^{-6}$s
Observation rate	$O_r = 0.5$
DOAs	$[-20, 10]^\circ$
Velocities	$[150, 450]$m/s
Powers of target reflection coefficient	$[0.3, 0.4]$
Number of Gaussian components	2
Probabilities of Gaussian components	$c_1 = 0.9, c_2 = 0.1$
Powers of Gaussian components	$10\sigma_1^2 = \sigma_2^2$
Proximal parameter	$\phi = 10^{-5}$
Maximum iteration number	50
Number of Monte-Carlo trials	250

of generality, assuming that $c_1 \gg c_2$ and $\sigma_1 \ll \sigma_2$, the first Gaussian component denotes the Gaussian background noise with small power σ_1^2 and large probability c_1, while the second denotes outliers with large power σ_2^2 and small probability c_2.

A. Convergence
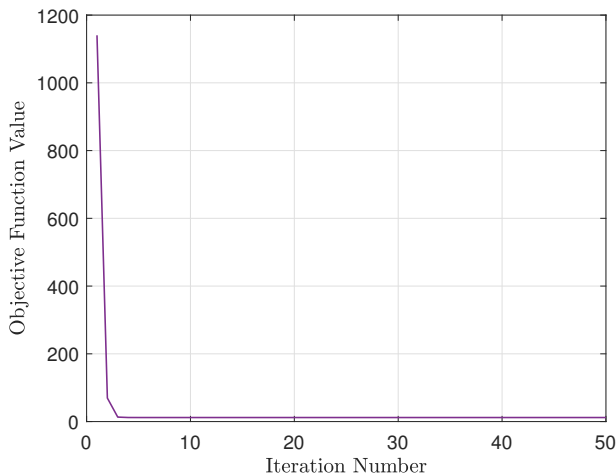
Fig. 2.   Illustration of Convergence.

Figure 2 provides the empirical evidence that Algorithm 1 converges. Here, the signal-to-noise ratio (SNR) is set as 10dB. We see that the objective function value is non-increasing as the iteration number increases, and becomes stable within three iterations.

Figures 3 and 4 show the convergence behaviors of the elements in U and V during iterations. The upper sub-figure depicts the real part and the lower one shows the imaginary
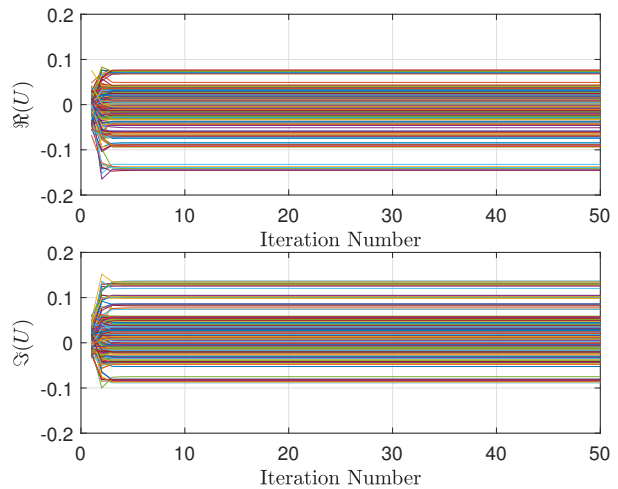
Fig. 3.   Convergence of elements in U.
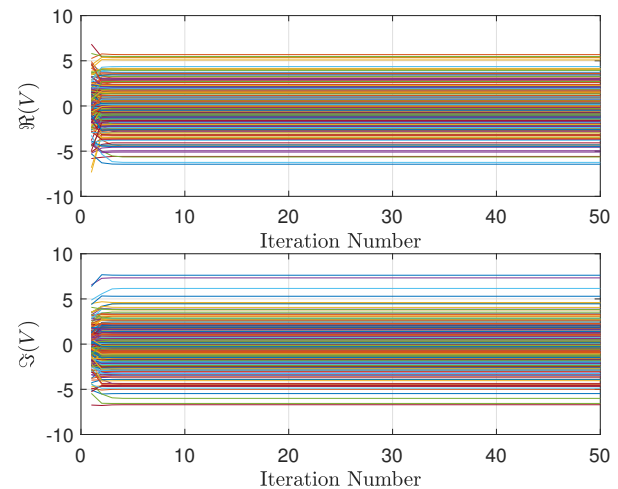
Fig. 4.   Convergence of elements in V.

part. Each line represents the value of one element versus the iteration number. We observe that each element in U and V converges after a few iterations, which confirms the convergence analysis in Section IV-A.

B. Pseudospectrum

Figures 5 and 6 illustrate the pseudospectrum output by the MUSIC algorithm in GMM and Gaussian noise, respectively. The SNR in this simulation is set as 10dB. The pseudospectrum is defined as the normalized power spectrum calculated as (9) in log scale, given by:

$$P_{pse}(\theta) = 10 \log \left(\frac{P(\theta)}{\max(P(\theta))} \right). \tag{41}$$

In both figures, all algorithms can successfully locate the targets at -20° and 10°. In GMM noise, thanks to the outlier detection and suppressing performance, the ℓ_0-norm minimization algorithm corresponds to the best spectral estimation because it has the largest relative peak among all approaches. In Gaussian noise, the proposed approach has
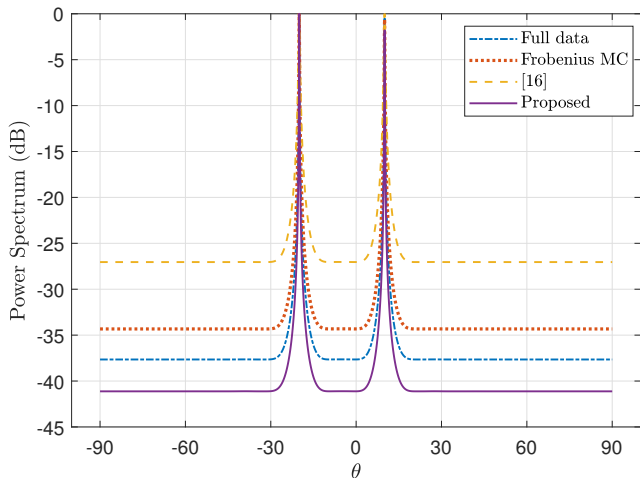
Fig. 5. Pseudospectrum in GMM noise.
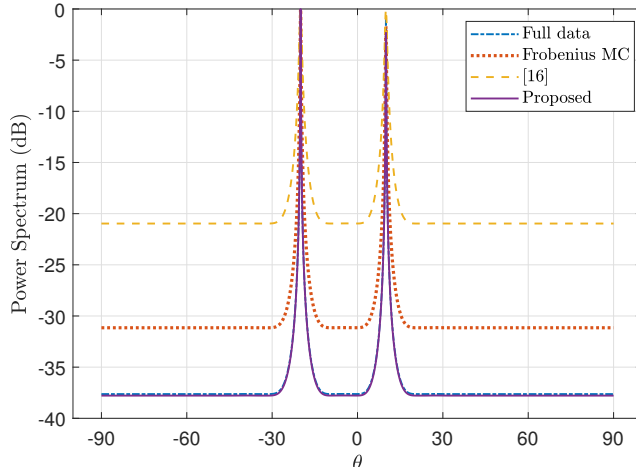
Fig. 7. Pseudospectrum in GMM noise, $O_r = 0.2$.
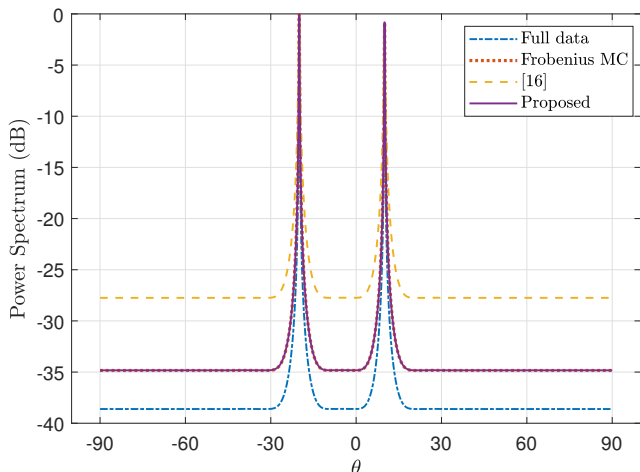
Fig. 6. Pseudospectrum in Gaussian noise.
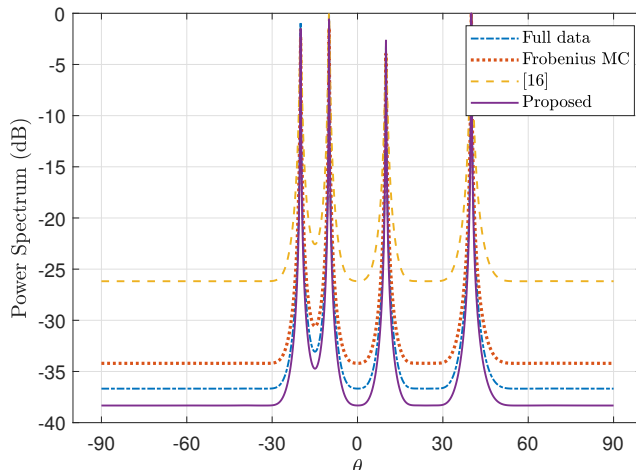
Fig. 8. Pseudospectrum in GMM noise, $K = 4$.

similar performance as the Frobenius norm based MC, and has better performance than [16]. Although full data sampling obtains the best performance in this case, its system loading is the largest.

Pseudospectrum computation in GMM noise under more harsh scenarios is investigated. Fig. 7 shows the performance of full-sampled system and MC based under-sampled system with an observation rate of 0.2, indicating that only 20% of the samples are collected. The penalty parameter μ is set as 8×10^{-3}. It is observed that the proposed method achieves the best spectral estimation among all MC algorithms. Furthermore, its performance with $O_r = 0.2$ is comparable to that of the full-sampling scheme. Fig. 8 shows the pseudospectrum for 4 targets located at $[-20, -10, 10, 40]°$. We see that our algorithm performs the best when the number of targets increases to 4, and is even superior to the full-sampling method.
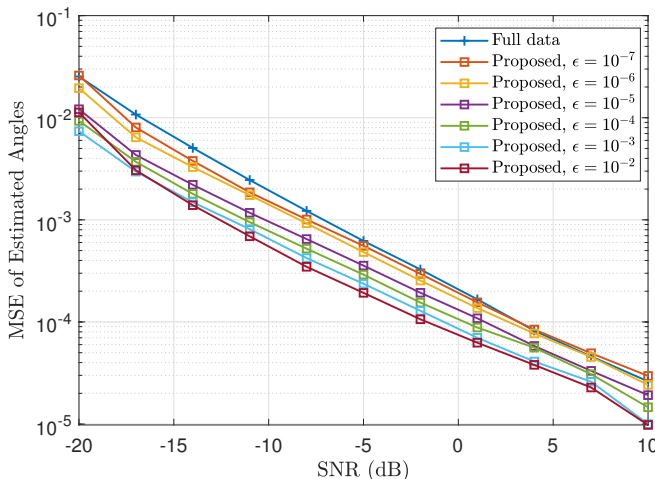
Fig. 9. MSE of estimated angles with different ϵ in GMM noise.

C. MSE of Estimated Angles

In Algorithm 1, the threshold of complex Laplacian kernel function is set as $\epsilon = 10^{-3}$. One may ask whether the performance is sensitive to the choice of ϵ, thus Fig. 9 is plotted to show the results using different values of ϵ in GMM noise. It is seen that when ϵ is smaller than 10^{-3}, the MSE of estimated angles becomes slightly larger. This is because when ϵ becomes smaller, less outliers are detected and suppressed, deteriorating the MSE performance. Although smaller ϵ leads to larger MSE, the MSE value is still lower than the MSE of full data, even if ϵ is set as an extremely small value, e.g. 10^{-7}.
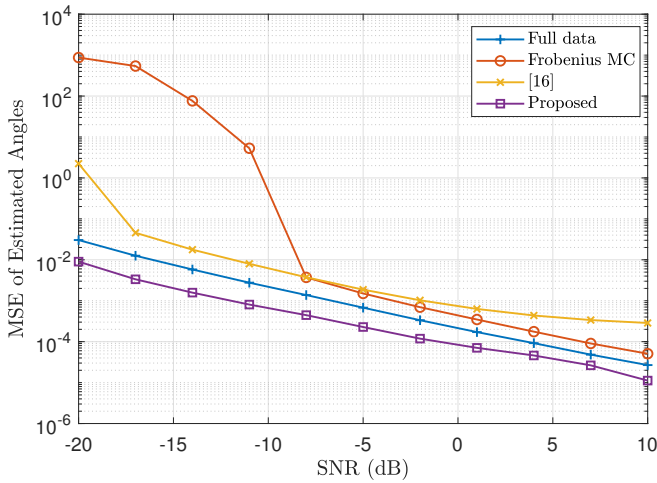
Fig. 10. MSE of estimated angles versus SNR in GMM noise.
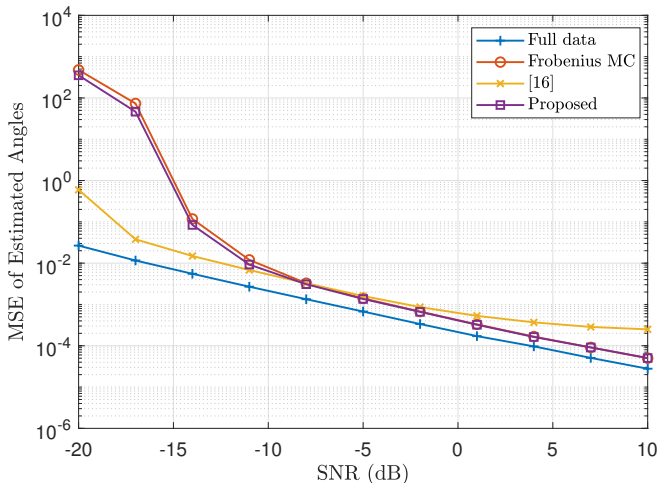
Fig. 11. MSE of estimated angles versus SNR in Gaussian noise.

Figures 10 and 11 show the MSE of estimated angles MSE_θ in GMM and Gaussian noise, respectively. MSE_θ is defined as:

$$\mathrm{MSE}_\theta = \mathbb{E}\left\{\left(\hat{\theta}_k - \theta_k\right)^2\right\} \tag{42}$$

where $\hat{\theta}_k$ is the estimated angle of the kth target. Similar to the result in pseudospectrum, the ℓ_0-norm minimization algo-

rithm has the smallest MSE in GMM noise. This is because the ℓ_0-norm minimization can detect and eliminate outliers. Moreover, the MUSIC algorithm used for target parameter estimation in MIMO radar can suppress the Gaussian noise, but not the outliers. Therefore, the under-sampled MIMO radar system with our ℓ_0-norm based approach achieves much higher robustness than the full-sampled MIMO radar system in impulsive noise. In Gaussian noise, the ℓ_0-norm minimization algorithm and the Frobenius norm based MC have similar performance, while [16] is better in the low SNR area and becomes worse when SNR is high. Since no outliers appear in the Gaussian noise and MUSIC algorithm can effectively handle the Gaussian noise, the MSE performance of the proposed system is similar to that of other systems.

D. Target Detection Probability
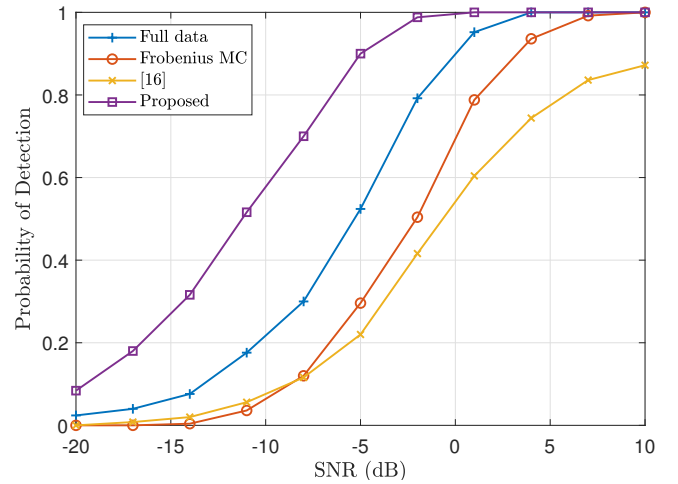
Fig. 12. Target detection probability versus SNR in GMM noise.
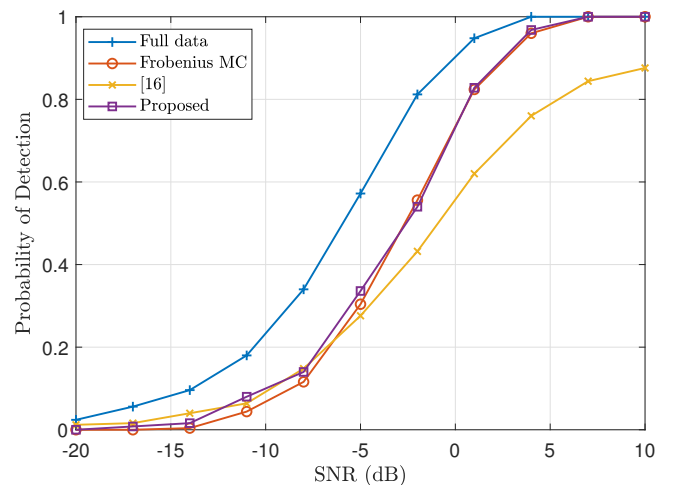
Fig. 13. Target detection probability versus SNR in Gaussian noise.

Figures 12 and 13 plot the target detection probability in GMM and Gaussian noise, respectively. The target detection

probability of 2 targets is defined as:

$$P_D = \text{Prob}\bigg(\left|\hat{\theta}_1 - \theta_1\right| < \delta \left|\theta_1 - \theta_2\right|$$
$$\text{and } \left|\hat{\theta}_2 - \theta_2\right| < \delta \left|\theta_1 - \theta_2\right| \bigg) \tag{43}$$

where δ denotes the tolerance of estimation errors, and $\delta = 10^{-3}$ is employed. In terms of target detection probability, the ℓ_0-norm minimization algorithm also has better performance in GMM noise. Moreover, it is observed from the Gaussian noise case that the MSE advantage of [16] in low SNR does not lead to high target detection probability, but the worse MSE performance of [16] in high SNR makes its target detection probability performance worse than the ℓ_0-norm minimization algorithm and the Frobenius norm based MC.

VI. CONCLUSION

A novel ℓ_0-norm minimization based MC approach for target localization in colocated MIMO radar is proposed in this paper. Aiming at reducing the sampling load, under-sampling is applied, leading to an incomplete matrix after sampling. Owing to the low-rank property of the noise-free colocated MIMO radar signal matrix, MC approach is applied to recover the complete matrix. To restrain outliers and Gaussian noise simultaneously, the proposed approach is formulated using a linear combination of Frobenius norm and ℓ_0-norm. The Frobenius norm is used for reducing the Gaussian noise while the ℓ_0-norm is used for detecting and resisting outliers. We adopt proximal BCD to decompose the problem into three subproblems which are alternately solved. Moreover, the complex Laplacian kernel with joint PDF of the real and imaginary parts and the median absolute deviation are applied to detect outliers. Convergence and complexity of the proposed approach are theoretically analyzed. Simulation results show that the ℓ_0-norm minimization based approach obtains superior pseudospectrum, MSE and target detection probability performances over the other MC-based approaches in GMM noise.

APPENDIX A
REASON OF CHOOSING THE SECOND SAMPLING SCHEME

We first explain why the first sampling scheme is not suitable. Since the first scheme performs the matched filtering prior to mixing the samples, the noise processed by the matched filter is:

$$\mathbf{\Xi}_q = \mathbf{W}_q \mathbf{S}^H \tag{44}$$

where the (b,a) element of $\mathbf{\Xi}_q \in \mathbb{C}^{M_r \times M_t}$ is $\xi_{b,a} = \sum_{n=1}^{N} w_{b,n} s_{a,n}$, $w_{b,n}$ is the (b,n) element of $\mathbf{W}_q$ and $s_{a,n}$ is the (a,n) element of $\mathbf{S}$. Suppose there is GMM impulsive noise, where the real and the imaginary parts have the same distribution. According to (40), the real part of the noise has the following distribution:

$$p_{\Re(w)}(\Re(w)) = \frac{c_1}{\sqrt{\pi}\sigma_1} e^{-\frac{\Re(w)^2}{\sigma_1^2}} + \frac{c_2}{\sqrt{\pi}\sigma_2} e^{-\frac{\Re(w)^2}{\sigma_2^2}}. \tag{45}$$

Then the characteristic function of $\Re(w)$ can be obtained by performing the Fourier transform on $p_{\Re(w)}(\Re(w))$, given by:

$$f_{\Re(w)}(t) = c_1 e^{-\frac{1}{4}(\sigma_1 t)^2} + c_2 e^{-\frac{1}{4}(\sigma_2 t)^2}. \tag{46}$$

Since $\mathbf{S}$ is part of the complex Hadamard matrix, (1) is used to determine the value of $s_{a,n}$, which implies that $s_{a,n} = \pm(1+j)/\sqrt{2N}$. Therefore, the real part of $\mathbf{\Xi}_q$ is:

$$\Re(\mathbf{\Xi}_q) = [\Re(\mathbf{W}_q) \quad \Im(\mathbf{W}_q)][\Re(\mathbf{S}) \quad \Im(\mathbf{S})]^T \tag{47}$$

where $\Re(\mathbf{S})$ and $-\Im(\mathbf{S})$ are matrices whose elements are $\pm 1/\sqrt{2N}$. Similarly, we know that the real and imaginary parts of $\xi_{b,a}$ have the same distribution. According to (46) and ignoring the subscripts b and a in $\xi_{b,a}$, the characteristic function of $\Re(\xi)$ is:

$$f_{\Re(\xi)}(t) = \left(c_1 e^{-\frac{1}{8N}(\sigma_1 t)^2} + c_2 e^{-\frac{1}{8N}(\sigma_2 t)^2} \right)^{2N}$$
$$= \sum_{m=0}^{2N} C_m^{2N} c_1^m c_2^{2N-m} e^{-\frac{m\sigma_1^2+(2N-m)\sigma_2^2}{8N}t^2}. \tag{48}$$

where C_m^{2N} denotes the number of m-combinations in $2N$ elements. Then the PDF of $\Re(\xi)$ is:

$$p_{\Re(\xi)}(\Re(\xi)) = \sum_{m=0}^{2N} \frac{C_m^{2N} c_1^m c_2^{2N-m}}{\sqrt{\pi}\nu_m} e^{-\frac{\Re(\xi)^2}{\nu_m^2}} \tag{49}$$

where

$$\nu_m^2 = \frac{m\sigma_1^2 + (2N-m)\sigma_2^2}{2N}. \tag{50}$$

In (49), the Gaussian component with variance $\sigma_1^2/2$ has the probability c_1^{2N}, and the Gaussian component with variance $\sigma_2^2/2$ has the probability c_2^{2N}. While in (45), the Gaussian component with variance $\sigma_1^2/2$ has the probability c_1, and the Gaussian component with variance $\sigma_2^2/2$ has the probability c_2. Comparing (49) and (45), the probabilities of Gaussian components with largest and smallest variances in (49) are much smaller than those in (45) because $0 < c_1, c_2 < 1$ and $2N \gg 1$. Therefore, we conclude that after the matched filtering in the first scheme, most of the noise power is concentrated on Gaussian components with variances between $\sigma_1^2/2$ and $\sigma_2^2/2$, which means that ξ is less impulsive than w. In other words, the matched filter averages the variance of different components, and makes the noise less impulsive. For other impulsive noise models, the noise after being processed by matched filter is also less impulsive, as the power difference of impulsive noise and background noise still exists. However, the robust MC techniques are more effective when the noise is more impulsive, thus these techniques should be applied in the original received data rather than the data after being processed by the matched filter in the first scheme. In the second scheme, MC is performed on the original received data, thus we choose it.

APPENDIX B
PROOF OF LOW RANK PROPERTY OF $\mathbf{Z}$

The MIMO radar transceiver uses a ULA configuration for both transmitter and receiver where the reflection coefficients

This article has been accepted for publication in IEEE Transactions on Aerospace and Electronic Systems. This is the author's version which has not been fully edited and content may change prior to final publication. Citation information: DOI 10.1109/TAES.2023.3280462

IEEE TRANSACTIONS ON AEROSPACE AND ELECTRONIC SYSTEMS 11

and Doppler spreads of targets are represented by diagonal matrices, $\boldsymbol{\Gamma}_q$ and $\boldsymbol{D}_q$, respectively. Subsequently, $\mathrm{vec}(\boldsymbol{Z}_q)$ is:

$$\mathrm{vec}(\boldsymbol{Z}_q) = \mathrm{vec}(\boldsymbol{B}\boldsymbol{\Gamma}_q\boldsymbol{D}_q\boldsymbol{A}^T\boldsymbol{S}) = \left((\boldsymbol{S}^T\boldsymbol{A}) \otimes \boldsymbol{B}\right)\mathrm{vec}(\boldsymbol{\Gamma}_q\boldsymbol{D}_q). \tag{51}$$

According to (6) and (51), $\boldsymbol{Z}$ is rewritten as:

$$\begin{aligned} \boldsymbol{Z} &= \left((\boldsymbol{S}^T\boldsymbol{A}) \otimes \boldsymbol{B}\right)[\mathrm{vec}(\boldsymbol{\Gamma}_1\boldsymbol{D}_1), \cdots, \mathrm{vec}(\boldsymbol{\Gamma}_Q\boldsymbol{D}_Q)] \\ &= \left((\boldsymbol{S}^T\boldsymbol{A}) \otimes \boldsymbol{B}\right)\boldsymbol{\Sigma} \end{aligned} \tag{52}$$

where $\boldsymbol{\Sigma} = [\mathrm{vec}(\boldsymbol{\Gamma}_1\boldsymbol{D}_1), \cdots, \mathrm{vec}(\boldsymbol{\Gamma}_Q\boldsymbol{D}_Q)]$. Since $\boldsymbol{\Gamma}_q\boldsymbol{D}_q$ is a $K \times K$ diagonal matrix, only the k^2th elements in $\mathrm{vec}(\boldsymbol{\Gamma}_q\boldsymbol{D}_q)$ are non-zero, where $k = 1, \cdots, K$. Therefore, only K rows in $\boldsymbol{\Sigma}$ are non-zero. Since $(\boldsymbol{S}^T\boldsymbol{A}) \otimes \boldsymbol{B} \in \mathbb{C}^{M_rN \times K^2}$ and $\boldsymbol{\Sigma} \in \mathbb{C}^{K^2 \times Q}$, $\boldsymbol{Z}$ is of low-rank when $M_r, N, Q \gg K$. $\boldsymbol{Z}_q$ and $\boldsymbol{Z}$ are low-rank matrices under the assumption that $M_r \gg K$, $N \gg K$, and $Q \gg K$, as stated in (4) and (52). This assumption is easily met by setting M_r, N, and Q to be sufficiently large. The low-rank property can be intuitively understood as a superimposition of signals from K paths, represented as K rank-1 sub-matrices.

REFERENCES

[1] I. Bekkerman and J. Tabrikian, "Target detection and localization using MIMO radars and sonars," *IEEE Trans. Signal Process.*, vol. 54, no. 10, pp. 3873–3883, Oct. 2006.

[2] L. Xu, J. Li, and P. Stoica, "Target detection and parameter estimation for MIMO radar systems," *IEEE Trans. Aerosp. Electron. Syst.*, vol. 44, no. 3, pp. 927–939, July 2008.

[3] S. M. Patole, M. Torlak, D. Wang, and M. Ali, "Automotive radars: A review of signal processing techniques," *IEEE Signal Process. Mag.*, vol. 34, no. 2, pp. 22–35, Mar. 2017.

[4] J. Li and P. Stoica, "MIMO radar with colocated antennas," *IEEE Signal Process. Mag.*, vol. 24, no. 5, pp. 106–114, Sept. 2007.

[5] T. Strohmer and B. Friedlander, "Compressed sensing for MIMO radar-algorithms and performance," in *2009 Conference Record of the Forty-Third Asilomar Conference on Signals, Systems and Computers*, Pacific Grove, CA, USA, Nov. 2009, pp. 464–468.

[6] Y. Yu, A. P. Petropulu, and H. V. Poor, "Measurement matrix design for compressive sensing-based MIMO radar," *IEEE Trans. Signal Process.*, vol. 59, no. 11, pp. 5338–5352, Nov. 2011.

[7] S. Gogineni and A. Nehorai, "Target estimation using sparse modeling for distributed MIMO radar," *IEEE Trans. Signal Process.*, vol. 59, no. 11, pp. 5315–5325, Nov. 2011.

[8] M. Rossi, A. M. Haimovich, and Y. C. Eldar, "Spatial compressive sensing for MIMO radar," *IEEE Trans. Signal Process.*, vol. 62, no. 2, pp. 419–430, Jan. 2014.

[9] D. Cohen, K. V. Mishra, D. Cohen, E. Ronen, Y. Grimovich, M. Namer, M. Meltsin, and Y. C. Eldar, "Sub-Nyquist MIMO radar prototype with Doppler processing," in *2017 IEEE Radar Conference*, Seattle, WA, USA, May 2017, pp. 1179–1184.

[10] D. Cohen and Y. C. Eldar, "Sub-Nyquist radar systems: Temporal, spectral, and spatial compression," *IEEE Signal Process. Mag.*, vol. 35, no. 6, pp. 35–58, Nov. 2018.

[11] D. Cohen, D. Cohen, Y. C. Eldar, and A. M. Haimovich, "SUMMeR: Sub-Nyquist MIMO radar," *IEEE Trans. Signal Process.*, vol. 66, no. 16, pp. 4315–4330, Aug. 2018.

[12] K. V. Mishra, Y. C. Eldar, E. Shoshan, M. Namer, and M. Meltsin, "A cognitive sub-Nyquist MIMO radar prototype," *IEEE Trans. Aerosp. Electron. Syst.*, vol. 56, no. 2, pp. 937–955, Apr. 2020.

[13] S. Sun, K. V. Mishra, and A. P. Petropulu, "Target estimation by exploiting low rank structure in widely separated MIMO radar," in *2019 IEEE Radar Conference*, Boston, MA, USA, Apr. 2019, pp. 1–6.

[14] S. Sun, A. P. Petropulu, and W. U. Bajwa, "Target estimation in colocated MIMO radar via matrix completion," in *2013 IEEE International Conference on Acoustics, Speech and Signal Processing*, Vancouver, BC, Canada, May 2013, pp. 4144–4148.

[15] D. S. Kalogerias and A. P. Petropulu, "Matrix completion in colocated MIMO radar: Recoverability, bounds & theoretical guarantees," *IEEE Trans. Signal Process.*, vol. 62, no. 2, pp. 309–321, 2014.

[16] S. Sun, W. U. Bajwa, and A. P. Petropulu, "MIMO-MC radar: A MIMO radar approach based on matrix completion," *IEEE Trans. Aerosp. Electron. Syst.*, vol. 51, no. 3, pp. 1839–1852, July 2015.

[17] S. Sun and A. P. Petropulu, "Waveform design for MIMO radars with matrix completion," *IEEE J. Sel. Top. Signal Process.*, vol. 9, no. 8, pp. 1400–1414, Dec. 2015.

[18] B. Li, A. P. Petropulu, and W. Trappe, "Optimum co-design for spectrum sharing between matrix completion based MIMO radars and a MIMO communication system," *IEEE Trans. Signal Process.*, vol. 64, no. 17, pp. 4562–4575, May 2016.

[19] B. Li and A. P. Petropulu, "Matrix completion based MIMO radars with clutter and interference mitigation via transmit precoding," in *2017 IEEE International Conference on Acoustics, Speech and Signal Processing*, New Orleans, LA, USA, Mar. 2017, pp. 3216–3220.

[20] X. Hu, N. Tong, J. Wang, S. Ding, and X. Zhao, "Matrix completion-based MIMO radar imaging with sparse planar array," *Signal Process.*, vol. 131, pp. 49–57, Feb. 2017.

[21] X. Hu, L. Zhang, J. Long, C. Liang, J. Liu, and Y. Wang, "High-resolution velocity-azimuth joint estimation for random-time-division-multiplexing multiple-input-multiple-output automotive radar using matrix completion," *IET Radar Sonar Navig.*, vol. 15, no. 10, pp. 1281–1296, Oct. 2021.

[22] K. C. Wiklundh, P. F. Stenumgaard, and H. M. Tullberg, "Channel capacity of Middleton's class A interference channel," *Electron. Lett.*, vol. 45, no. 24, pp. 1227–1229, Dec. 2009.

[23] G. Laguna-Sanchez and M. Lopez-Guerrero, "On the use of alpha-stable distributions in noise modeling for PLC," *IEEE Trans. Power Del.*, vol. 30, no. 4, pp. 1863–1870, Aug. 2015.

[24] F. Pascal, P. Forster, J.-P. Ovarlez, and P. Larzabal, "Performance analysis of covariance matrix estimates in impulsive noise," *IEEE Trans. Signal Process.*, vol. 56, no. 6, pp. 2206–2217, June 2008.

[25] W.-J. Zeng, H. C. So, and L. Huang, "ℓ_p-MUSIC: Robust direction-of-arrival estimator for impulsive noise environments," *IEEE Trans. Signal Process.*, vol. 61, no. 17, pp. 4296–4308, Sept. 2013.

[26] W.-J. Zeng and H. C. So, "Outlier-robust matrix completion via ℓ_p-minimization," *IEEE Trans. Signal Process.*, vol. 66, no. 5, pp. 1125–1140, Mar. 2018.

[27] N. Rožić, P. Banelli, D. Begušić, and J. Radić, "Multiple-threshold estimators for impulsive noise suppression in multicarrier communications," *IEEE Trans. Signal Process.*, vol. 66, no. 6, pp. 1619–1633, Mar. 2018.

[28] Z. Yu, J. Li, Q. Guo, and T. Sun, "Message passing based robust target localization in distributed MIMO radars in the presence of outliers," *IEEE Signal Process. Lett.*, vol. 27, pp. 2168–2172, Dec. 2020.

[29] A. B. Baral and M. Torlak, "Joint Doppler frequency and direction of arrival estimation for TDM MIMO automotive radars," *IEEE J. Sel. Top. Signal Process.*, vol. 15, no. 4, pp. 980–995, June 2021.

[30] U. K. Singh, R. Mitra, V. Bhatia, and A. K. Mishra, "Kernel minimum error entropy based estimator for MIMO radar in non-Gaussian clutter," *IEEE Access*, vol. 9, pp. 125 320–125 330, Sept. 2021.

[31] E. Kim, Y. Yamada, and O. Shogo, "Robust asymmetric safety Kalman filter for MIMO radar resisting temporary outliers," *IEEE Sens. J.*, Aug. 2022.

[32] J. Li and P. Stoica, *MIMO Radar Signal Processing*. John Wiley & Sons, 2008.

[33] E. Fishler, A. Haimovich, R. Blum, L. Chizhik, L. Cimini, and R. Valenzuela, "MIMO radar: An idea whose time has come," in *Proceedings of the 2004 IEEE Radar Conference*, Philadelphia, PA, USA, Apr. 2004, pp. 71–78.

[34] L.-T. Huang, A. L. De Almeida, and H. C. So, "Target estimation in bistatic MIMO radar via tensor completion," *Signal Process.*, vol. 120, pp. 654–659, Mar. 2016.

[35] T. Aittomaki and V. Koivunen, "Performance of MIMO radar with angular diversity under Swerling scattering models," *IEEE J. Sel. Top. Signal Process.*, vol. 4, no. 1, pp. 101–114, Feb. 2010.

[36] H. L. Van Trees, *Optimum Array Processing*. John Wiley & Sons, 2002.

[37] A. Bunse-Gerstner, "Matrix factorizations for symplectic QR-like methods," *Linear Algebra Appl.*, vol. 83, pp. 49–77, Nov. 1986.

[38] M. T. Chu, R. E. Funderlic, and G. H. Golub, "A rank-one reduction formula and its applications to matrix factorizations," *SIAM rev.*, vol. 37, no. 4, pp. 512–530, Dec. 1995.

[39] R. Zdunek and A. Cichocki, "Nonnegative matrix factorization with constrained second-order optimization," *Signal Process.*, vol. 87, no. 8, pp. 1904–1916, Aug. 2007.

[40] F. Wen, R. Ying, P. Liu, and T.-K. Truong, "Nonconvex regularized robust PCA using the proximal block coordinate descent algorithm," *IEEE Trans. Sig. Process.*, vol. 67, no. 20, pp. 5402–5416, Oct. 2019.

This article has been accepted for publication in IEEE Transactions on Aerospace and Electronic Systems. This is the author's version which has not been fully edited and content may change prior to final publication. Citation information: DOI 10.1109/TAES.2023.3280462

IEEE TRANSACTIONS ON AEROSPACE AND ELECTRONIC SYSTEMS   12

[41] J. Kim and C. D. Scott, "Robust kernel density estimation," *J. Mach. Learn. Res.*, vol. 13, no. 1, pp. 2529–2565, Jan. 2012.

[42] A. M. Zoubir, V. Koivunen, E. Ollila, and M. Muma, *Robust Statistics for Signal Processing*. Cambridge University Press, 2018.

[43] B.-Z. Li, X.-L. Zhao, J.-L. Wang, Y. Chen, T.-X. Jiang, and J. Liu, "Tensor completion via collaborative sparse and low-rank transforms," *IEEE Trans. Comput. Imaging*, vol. 7, pp. 1289–1303, Nov. 2021.

[44] J. Bolte, S. Sabach, and M. Teboulle, "Proximal alternating linearized minimization for nonconvex and nonsmooth problems," *Math. Program.*, vol. 146, no. 1, pp. 459–494, Aug. 2014.

[45] H. Attouch, J. Bolte, and B. F. Svaiter, "Convergence of descent methods for semi-algebraic and tame problems: Proximal algorithms, forward–backward splitting, and regularized Gauss–Seidel methods," *Math. Program.*, vol. 137, no. 1-2, pp. 91–129, 2013.

[46] Q. Liu, X. Li, H. Cao, and Y. Wu, "From simulated to visual data: A robust low-rank tensor completion approach using ℓ_p-regression for outlier resistance," *IEEE Trans. Circuits Syst. Video Technol.*, vol. 32, no. 6, pp. 3462–3474, 2022.
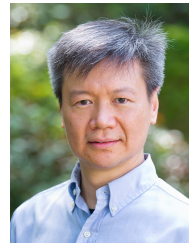
Hing Cheung So (S'90–M'95–SM'07-F'15) was born in Hong Kong. He received the B.Eng. degree from the City University of Hong Kong and the Ph.D. degree from The Chinese University of Hong Kong, both in electronic engineering, in 1990 and 1995, respectively. From 1990 to 1991, he was an Electronic Engineer with the Research and Development Division, Everex Systems Engineering Ltd., Hong Kong. During 1995–1996, he was a Postdoctoral Fellow with The Chinese University of Hong Kong. From 1996 to 1999, he was a Research Assistant Professor with the Department of Electronic Engineering, City University of Hong Kong, where he is currently a Professor. His research interests include detection and estimation, fast and adaptive algorithms, multidimensional harmonic retrieval, robust signal processing, source localization, and sparse approximation.

He has been on the editorial boards of IEEE Signal Processing Magazine (2014–2017), IEEE Transactions on Signal Processing (2010–2014), Signal Processing (2010–), and Digital Signal Processing (2011–). He was also Lead Guest Editor for IEEE Journal of Selected Topics in Signal Processing, special issue on "Advances in Time/Frequency Modulated Array Signal Processing" in 2017. In addition, he was an elected member in Signal Processing Theory and Methods Technical Committee (2011–2016) of the IEEE Signal Processing Society where he was chair in the awards subcommittee (2015–2016).

Zhaofeng Liu received the B.S. and M.S. degrees both in School of Electronics and Information Technology from Sun Yat-sen University, Guangzhou, China, in 2018 and 2020, respectively. He is currently pursuing the Ph.D. degree in Department of Electrical Engineering, City University of Hong Kong. His research interests include chaotic communication, multi-carrier modulation, robust signal processing, and MIMO radar.

Xiao Peng Li received the B.Eng. degree in electronic science and technology from Yanshan University, Qinhuangdao, China, in 2015, and the M.Sc. degree (with Distinction) in electronic information engineering and the Ph.D. degree in electrical engineering from the City University of Hong Kong, Hong Kong, SAR, China, in 2018 and 2022, respectively.

He was a Research Assistant with the Department of Information Engineering, Shenzhen University, Shenzhen, China, from 2018 to 2019, and a Postdoctoral Fellow with the Department of Electrical Engineering, City University of Hong Kong from 2022 to 2023. He is currently an Assistant Professor with the College of Electronics and Information Engineering, Shenzhen University. His research interests include optimization methods, machine learning, sparse recovery, matrix processing and tensor processing with applications in target estimation, image recovery, video restoration, hyperspectral unmixing, and stock market analysis.